JET-P(95)42

JET Results with the New Pumped Divertor and Implications for ITER

The JET Team

presented by M Keilhacker.

JET Joint Undertaking, Abingdon, Oxfordshire, OX14 3EA, UK.

Preprint of an Invited paper submitted for publication in a special issue of Controlled Fusion and Plasma Physics

August 1995

JET Results with the New Pumped Divertor and Implications for ITER

The JET Team[§]
(presented by M Keilhacker)
JET Joint Undertaking, Abingdon, Oxon, OX14 3EA, UK

Abstract. This paper presents an overview of results of the 1994/95 experimental campaign on JET with the new pumped divertor and draws implications for ITER in the areas of detached and radiative divertor plasmas, the use of beryllium as a divertor target tile material, the confinement properties of discharges with the same dimensionless parameters (except for the dimensionless Larmor radius) as ITER and the effect of varying the toroidal magnetic field ripple in the ITER relevant range. Discharges with high fusion performance at high current, in steady-state with ELMs and in the ELM-free hot -ion H-mode, are also reported. Limits to operations are discussed and projections to D-T performance are made.

1. Introduction

After extensive modifications, JET became operational at the beginning of 1994. During the ensuing 1994/95 experimental campaign, the plasma current was increased to 6MA, the total heating power to 32MW, the plasma stored energy to 13.5MJ and the neutron rate to 4.7×10^{16}neutrons/s. The power handling, heating, pumping and high current capabilities of the New JET have been fully demonstrated and this has allowed a full programme in support of ITER [1] to be carried out. JET results are particularly important for ITER because of JET's large physical size, ITER-like plasma geometry and divertor configuration, and proximity to ITER plasma conditions.

The paper is organised as follows. The power handling, heating, pumping and high current capabilities of the new JET pumped divertor are discussed in Section 2. Experiments with detached and radiative divertor plasmas are reported in Section 3 and implications for ITER are drawn (as also in Ssections 4 - 6). Operation after the CFC divertor target tiles were replaced by beryllium tiles is discussed in Section 4, including a controlled beryllium melt experiment for ITER. Studies of the H-mode threshold power and energy confinement (including ρ^* scaling of ELMy H-modes) are reported in Section 5, and fast particle studies involving varying the toroidal magnetic field ripple and exciting and detecting Alfvén eigenmodes are set out in Section 6. High fusion performance plasmas are discussed in Section 7 and the summary and conclusions follow in Section 8.

2. The new JET pumped divertor

2.1. Power handling capability

Power handling with the new target structure is vastly improved over the roof-top X-point protection tiles which were mounted directly on the vacuum vessel for the 1991/92 experimental campaign. The careful attention paid to the present design and installation of

§ See Appendix I

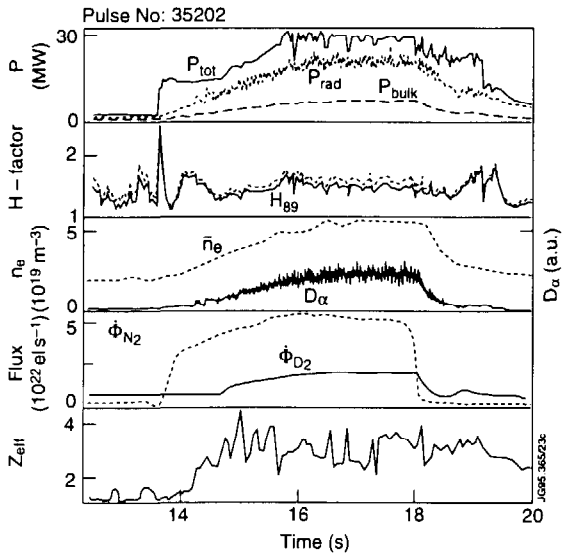

Figure 1. H-mode discharge in which most of the power is exhausted by radiation from seeded nitrogen with 30MW of combined (NBI and ICRF) heating

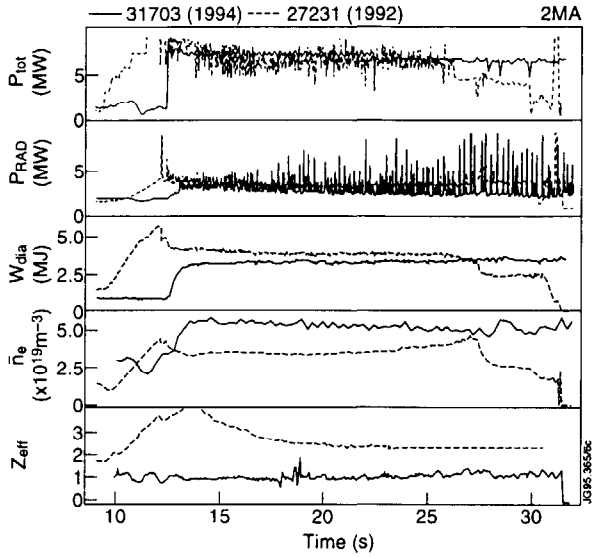

Figure 2. Comparison of similar discharges, one pumped (from 1994) and one unpumped (from 1992), showing effect of pumping in steady-state H-mode plasmas

the unidirectional tiles completely eliminates exposed edges and this has resulted in elimination of the carbon "bloom", often encountered in the past. For high energy pulses, "sweeping" the magnetic configuration over the divertor target tiles at 4Hz is used to limit tile temperatures well below those at which significant sublimation or melting can occur. As a result, energies conducted to the horizontal target plates have exceeded 100MJ with both CFC and beryllium tiles with no sign of damage.

2.2. High power, steady state H-mode plasmas with radiative power exhaust

JET has successfully established quasi-steady H-mode plasmas with combined (NBI and ICRF) heating powers up to 32MW. Most of the power was exhausted by radiation from seeded impurities. This result is of great importance to ITER, which relies on such a method of power exhaust [2]. Figure 1 shows a discharge which uses nitrogen seeding and additional deuterium fuelling. The radiated power is ~75% of the input power, with two thirds of the radiation emanating from below the X-point. The H-mode quality factor relative to the ITER89P database is about 1.5. Figure 1 also shows that the density reaches a steady value, and the D_α signal shows the presence of benign "grassy" ELMs. In discharges of this type, total deposited energies up to 180MJ (120MJ) have been used with CFC (beryllium) tiles.

2.3. H-mode density control using the cryopump

It is well known that density control is very difficult in H-modes at a given plasma current. In the new JET, the divertor cryopump allows good density control. By varying the separatrix strike point location relative to the outer corner of the divertor (where the conductance to the pump is largest), the pumping rate can be varied by a factor of about two. When used in conjunction with varying amounts of NBI and gas fuelling, it is possible to vary the plasma density in steady-state by a factor greater than 1.5.

The cryopump makes possible longer, cleaner, and more stationary H-modes with n_e, Z_{eff}, P_{rad}, and W_{dia} remaining constant for up to 20s (~$40\tau_E$). This is illustrated in figure 2, which compares a pumped (from 1994) and an unpumped (from 1992) 2MA discharge with otherwise

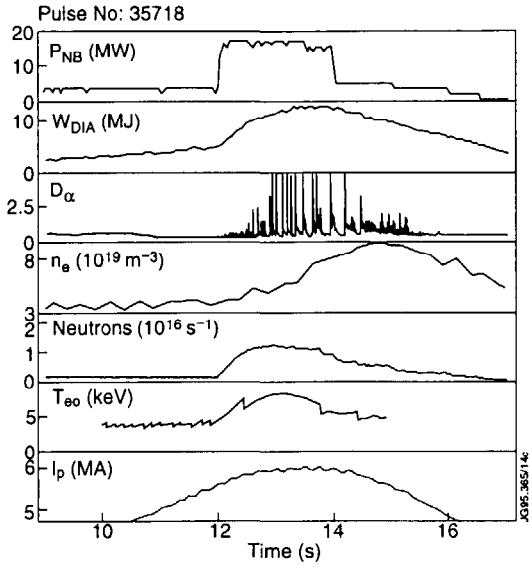

Figure 3. ELMy H-mode discharge at 6MA plasma current and with 18MW of NB heating

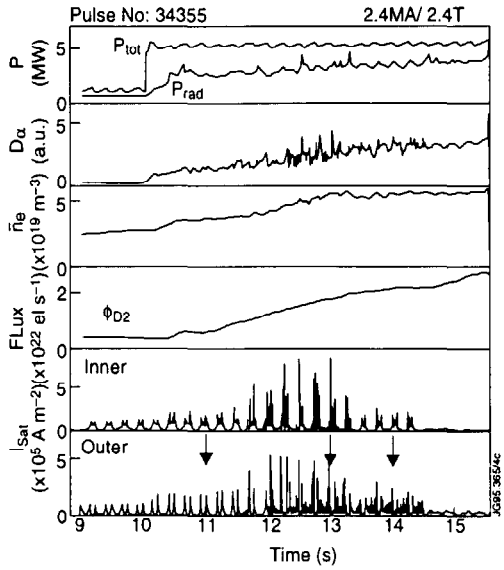

Figure 4. L-mode discharge where detachment of plasma from divertor target is obtained by deuterium puffing with intrinsic impurities only

identical parameters. Note the ELMy nature of the 1994 discharge, which is characteristic of H-modes in the new JET.

2.4. High current 6MA H-mode plasmas

The full 6MA current capability of JET has also been demonstrated [3] and 6MA H-modes have been obtained with up to 18MW of NBI heating (figure 3). The beneficial current dependence in ELMy H-modes has been demonstrated for currents up to 6MA [3].

3. Detached and radiative divertor plasmas

At the beginning of the ITER EDA, it was realised that conventional high recycling divertor operation would result in target heat loads higher than those which could be accommodated without target melting or vaporization. This led to the proposal [2,4] of a detached, highly radiating divertor plasma in which the exhaust power is distributed, by radiation and charge-exchanged neutral losses, over the divertor sidewalls, which have a sufficiently large area to reduce the heat load to acceptable values. At JET, the investigation of such divertor plasmas began in 1992, and has been pursued in depth with the Mark I divertor [5].

3.1. Detachment with intrinsic impurities only

Figure 4 shows data from a detached L-mode discharge without impurity seeding. As fuelling by deuterium is increased, the radiated power fraction increases to about 70% and the density increases to a steady value of about $5x10^{19}m^{-3}$. The two lower boxes show the particle flow to the inner and outer targets as measured by Langmuir probes. The 4Hz modulation is due to sweeping, while the envelope shows the peak values on the target at the separatrix. It can be seen that as the plasma density rises, the particle flux at the target first increases (high recycling), then levels off ("rollover"), and finally decreases (detachment). The temperature (not shown) also decreases, so that both the heat flux and pressure at the target decrease. This is illustrated in figure 5, which shows profiles of electron pressure at the midplane and along the target, mapped to midplane distances, for the three times indicated by the arrows on figure 4. It can be seen that a

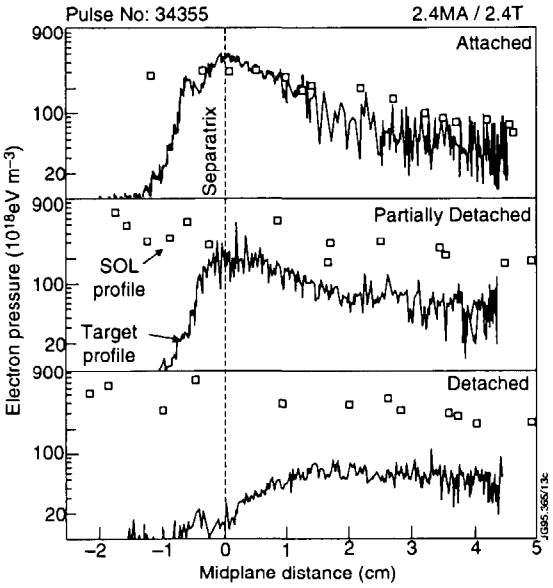

Figure 5. Evolution of parallel electron pressure gradient between the midplane and divertor target at the three times marked in figure 4

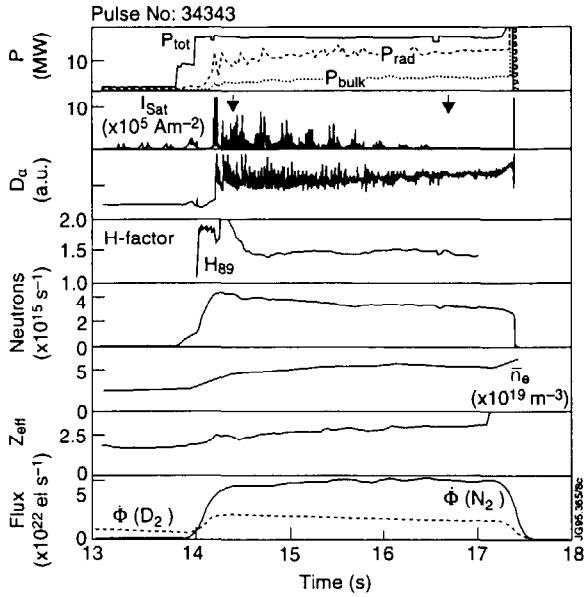

Figure 6. H-mode discharge in which a radiative detached divertor plasma is established by nitrogen seeding

significant pressure drop (more than a factor of 10 near the separatrix) develops between midplane and target, a signature of detachment.

3.2. Detached radiative divertor H-mode plasmas

It has not been possible to produce detached divertor plasmas with H-mode confinement in JET by using deuterium fuelling alone. This had been predicted theoretically for both JET [6] and ITER [7]. At the powers required to maintain the H-mode, the density required to reduce the divertor temperature to the point where detachment can occur (below 5eV) exceeds the H-mode density limit, and a transition back to the L-mode occurs. H-mode detached plasmas can, however, be produced by introducing an impurity into the divertor to enhance radiation. Neon, nitrogen, and argon seeds have been injected into JET, either pre-programmed or feedback-controlled on the divertor radiation or the ion saturation current at the targets. It has been seen that nitrogen radiates more in the divertor, while neon and argon require lower influxes. Preliminary indications are that argon produces the lowest dilution in the plasma core for a given radiated power fraction.

Figure 6 shows a nitrogen seeded discharge, which is also fuelled by deuterium in the main chamber to replenish the particles removed by the cryopump and to produce a particle flow in the scrape-off layer. Following the "rollover", the radiated power fraction rises to more than 85%, with two-thirds of this in the divertor. The H-factor levels off at about 1.5, typical of detached H-mode discharges in JET. Z_{eff} rises to about 2.5, somewhat lower than found with neon seeds. Figure 7 shows tomographic reconstructions of the radiation pattern in the lower half of the vacuum vessel as measured by a bolometer array [8]. At 14.4s, when the plasma is partially detached, the radiation is well distributed throughout most of the divertor volume below the X-point. In this case, there is still some power flux to the target, but it is quite low. Z_{eff} is also somewhat lower than at later times. At 16.7s, the radiating volume has moved away from the targets and is located at the X-point, with some fraction of the radiation emanating from inside the separatrix. The motion of the radiating volume is smooth, but occurs over a fairly small range of total radiated power. Similar behaviour is predicted using the full multispecies EDGE2D/NIMBUS code system at JET [9].

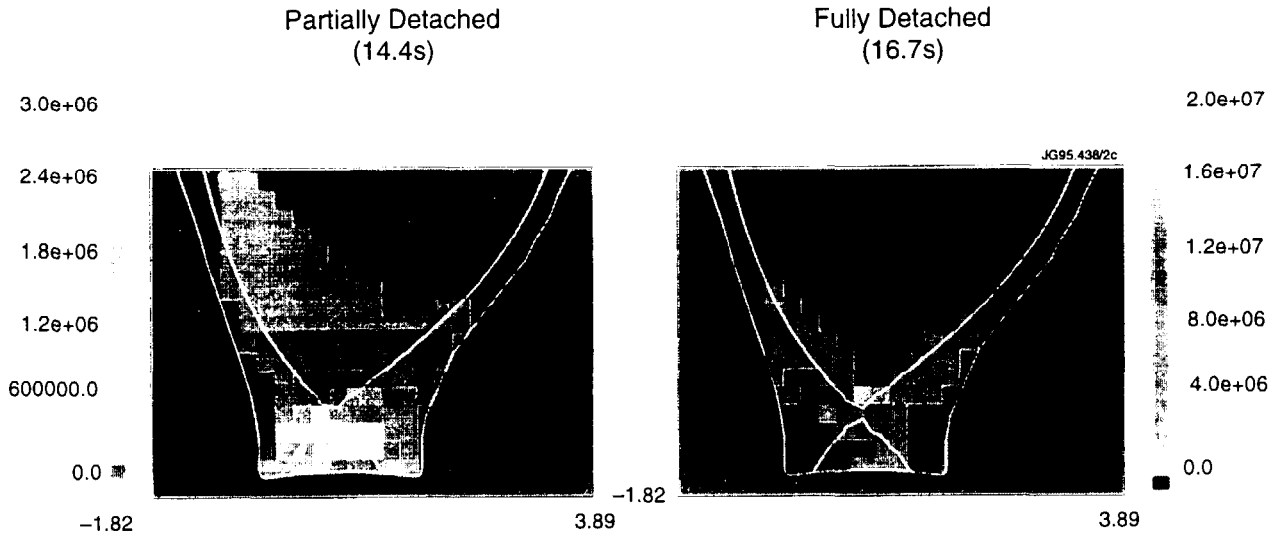

Figure 7. Tomographic reconstruction of radiation pattern in lower half of the vessel during partially (at 14.4s) and fully (at 16.7s) detached phases of the discharge of figure 6 showing the radiating zone moving smoothly from the target to the X-point region

3.3. Implications for ITER

The results reported here are quite promising for ITER [10]. The achieved radiated power fractions of 80% to 85% are sufficient to prevent target damage, overheating and erosion. The achieved H-factor would be sufficient for ignition in ITER. Detachment is accompanied by a transition from large isolated ELMs to more benign "grassy" ELMs which should not cause target damage. There is somewhat more of a problem with main plasma impurity contamination from the impurity seed. The observed concentrations would be barely acceptable in ITER with argon, and are clearly too high with either neon or nitrogen. The scaling from JET to ITER has, however, yet to be established. In JET, improvements might arise with the more closed divertor geometries, which are scheduled for introduction in two stages: operation with Mark IIA is expected to start early in 1996, followed by Mark II Gas Box operation in the middle of 1997.

4. Beryllium target tile assessment

For the last three months of the 1994/95 experimental campaign, the CFC divertor target tiles were replaced by beryllium tiles of similar geometry and a full experimental programme was carried out to compare CFC and beryllium as a plasma facing material. The campaign was concluded by exposing the target to significantly higher heat fluxes, with the explicit aim of studying the behaviour of molten and damaged beryllium [11].

4.1. Performance under normal operating conditions

Under normal operating conditions, the power handling capabilities of the CFC and beryllium target were found to be comparable, with similar deposited energies (~100MJ). Figure 8 shows that long pulse steady-state H-modes with similar characteristics could be established on either carbon or beryllium. The carbon concentrations in the plasma were lower with beryllium tiles, although impurity radiation was still dominated by carbon. This may be due to impurities from the poloidal carbon limiters and wall protection tiles and may account for the very similar behaviour in the two cases. For example, the H-mode power threshold including its scaling with toroidal magnetic field and density, was the same with CFC or

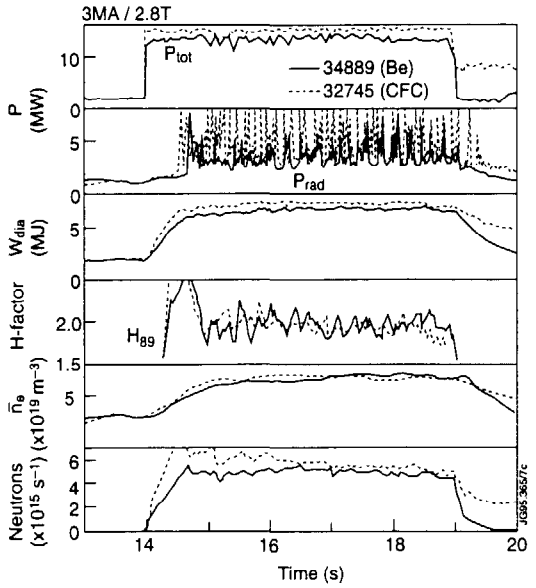

Figure 8. Pulse characteristics of two similar steady-state H-mode discharges showing that under normal operating conditions the general plasma behaviour is remarkably similar for operation on beryllium or CFC target tiles

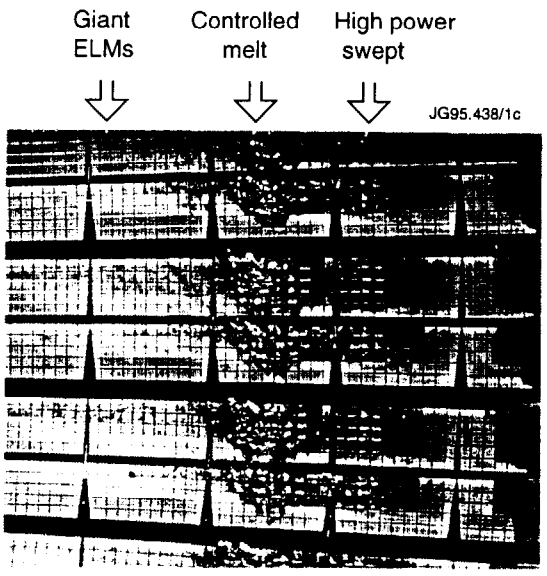

Figure 9. Photograph of a sector of the outer divertor target, showing some damage caused by "giant" ELMs, high power swept operation and the controlled melt experiment

beryllium tiles. Behaviour at the density limit was the same, with little margin between detachment and the density limit. The density range for detachment was also very similar and plasma fuelling and exhaust rates differed very little. H-mode confinement was lost when the radiated power fraction reached ~50% with intrinsic impurities, and detached H-modes (radiated power fraction ~80%) could only be achieved with impurity seeding.

4.2. Effect of giant ELMs and disruptions

Gross melting of the target tiles was generally avoided by limiting the input energy and by "sweeping". Superficial melt damage (figure 9) was made, however, by some giant ELMs in hot-ion H-mode discharges. Each ELM deposited about 1MJ of plasma energy onto the target in about 20ms (figure 10). This is much shorter than the sweep period of 0.25s and the heat is therefore deposited locally.

Several density limit disruptions also occurred, but did not lead to melting of the beryllium. The maximum target temperature measured just after a disruption did not exceed about 800°C (the beryllium melting temperature is 1280°C). However, this result may not be representative of other types of disruptions.

4.3. Effect of molten beryllium surfaces

JET has also tested the hypothesis put forward by ITER [12] that a beryllium target would 'self-protect' against excessive heat fluxes during abnormal events by evaporated beryllium from solid and slightly molten targets leading to high radiation from the plasma and reduced heat fluxes.

JET experiments were nominally at the ITER reference heat fluxes of 25MW/m^2 [10], but only a moderate degree of self-protection of the beryllium target was found. Despite significant surface melting, the radiated power rarely exceeded 50% of the input power, although in some discharges, at low density and without additional gas fuelling, it increased to ≈70% after several seconds. The target had melted to a depth of 2 to 3mm near the outer strike point. This damage is also marked in figure 9.

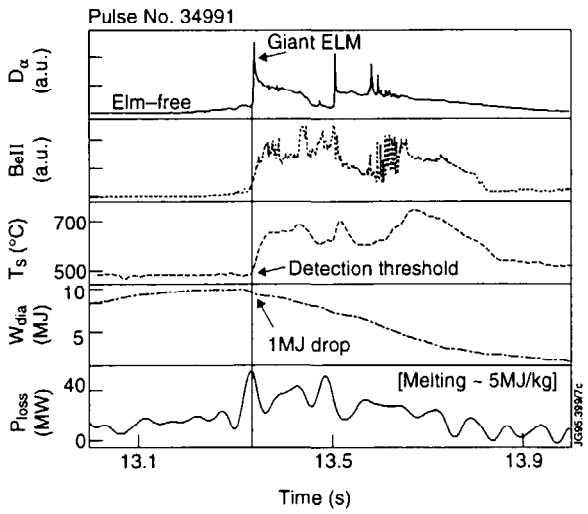

Figure 10. Pulse characteristics showing that a "giant" ELM (dumping 1MJ in <20ms) leads to surface melting at the target plates, despite "sweeping"

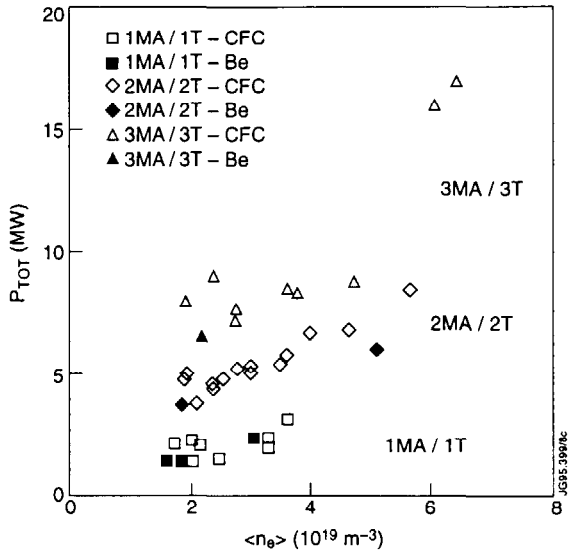

Figure 11. H-mode threshold power versus density at 1MA/1T, 2MA/2T and 3MA/3T and with CFC and beryllium targets

Following these experiments, operation with the strike points located on melted beryllium was attempted. Gas-fuelled ELMy H-mode discharges and nitrogen seeded radiative divertor discharges were essentially unchanged, but low density H-mode discharges without gas fuelling showed degraded performance. Operation with sweeping over the damaged region could be recovered after a few conditioning discharges. Subsequently, in high power swept operation, 180MJ of input energy was deposited on the target, causing additional melting (figure 9).

4.4. Implications for ITER

Under normal operating conditions gross melting damage to the tiles was avoided by careful operation, although some superficial damage was produced by giant ELMs. Significant tile damage has been inflicted during a controlled melt experiment when ITER reference heat fluxes of 25MW/m^2 were applied and only a moderate degree of self-protection of the beryllium target was found. Following melting, the effect of a damaged beryllium target on the operating regimes relevant to ITER was found to be small. All in all, beryllium remains one of the candidate plasma facing materials for ITER and the final choice will depend largely on other considerations such as co-deposition and tritium retention.

5. H-mode threshold power and energy confinement

JET has been a major contributor to the multi-machine scaling studies for ITER on the H-mode threshold power and transport in steady-state ELMy H-modes.

5.1. H-mode threshold power

The transition to the high confinement H-mode has been achieved with similar powers to those required during previous experimental campaigns. A more thorough study has now been carried out [13] and, when combined with results from other tokamaks operated with the same geometry, a more accurate size scaling of the threshold power will be determined and used in predictions for ITER.

The H-mode threshold power in 1MA/1T, 2MA/2T, 3MA/3T discharges with the ITER geometry and ITER value of the edge safety factor, q_{95}=3, is shown over a wide range of densities in figure 11. As can be seen, the threshold power is similar for CFC and beryllium

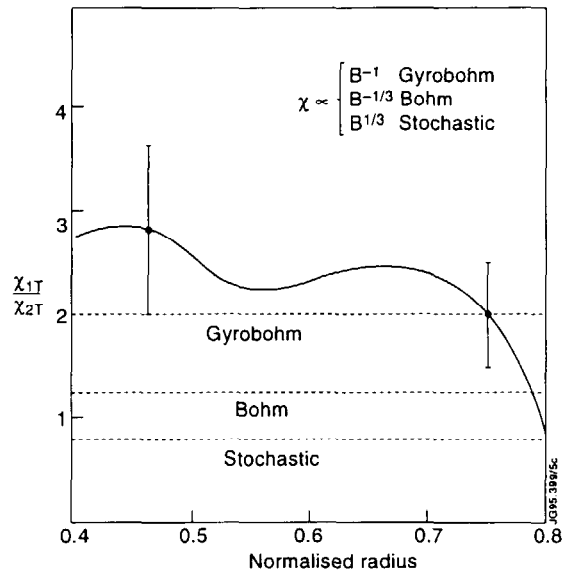

Figure 12. Thermal diffusivities in the ELMy H-mode discharges (at 1MA/1T and 2MA/2T) of ρ* scaling experiments showing a scaling close to gyrobohm

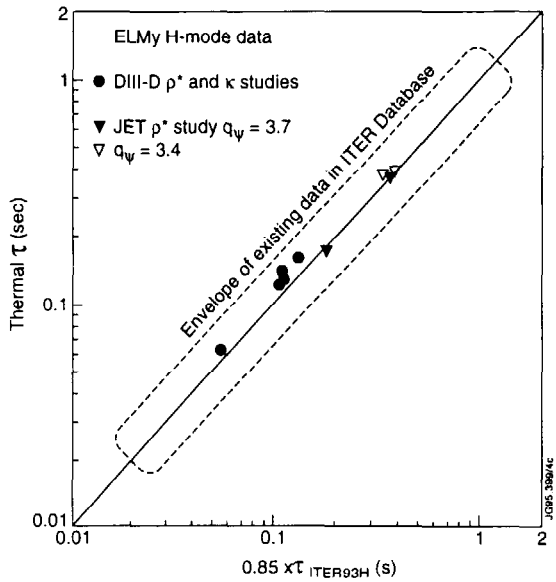

Figure 13. JET ρ* scaling data of ELMy H-mode energy confinement extend DIII-D data towards ITER values and show a quasi-gyrobohm scaling (0.85 x ITER93H)

targets. A regression analysis shows that the H-mode threshold power varies as $n_e^{0.74}B^{1.1}$ [13], which is similar to the dimensionally correct scaling $n_e^{0.75}BL^2$ which is one of the forms which gives a reasonable fit to the H-mode threshold data base [14]. Although the dependence on the toroidal magnetic field is very clear in figure 11, the dependence on density is less clear both at high and low density, where there is clear evidence of a departure from a simple $n^{0.75}$ dependence, particularly in the 3MA/3T data.

5.2. Confinement in ELMy H-modes

ELMy H-mode plasmas with steady conditions for many energy confinement times are considered the most credible mode of operation for ITER. After a period free of ELM instabilities, plasmas in the new JET configuration develop regular ELMing behaviour, with confinement typically a factor H≈1.8 higher than low confinement (L-mode) scalings, such as ITER89P.

Larmor radius scaling experiments have been conducted in ELMy H-modes [15]. These similarity experiments, which form part of the multi-machine scaling studies for ITER, keep all dimensionless parameters (β, ν*, q, ε, κ, etc) constant except for the dimensionless Larmor radius, $\rho^* = \rho_i/L$.

Pairs of discharges at 1MA/1T and 2MA/2T, which are well above the H-mode threshold power, have thermal diffusivities which show a scaling close to gyrobohm (figure 12). These JET experiments extend DIII-D studies [16,17] towards ITER and confirm the quasi-gyrobohm expression of the ITER93H H-mode scaling (figure 13). It should be noted, however, that gyrobohm scaling holds only for power levels well above the H-mode threshold, while close to the threshold, the scaling becomes Bohm or Goldston-like with the power scaling following that of the threshold (figure 14).

5.3. Implications for ITER

The JET and DIII-D ρ* scaling data can be interpreted in terms of gyrobohm scaling which is degraded as the H-mode threshold power is approached. Since ITER is foreseen to operate close to the threshold, multi-machine scaling studies for ITER should now aim to provide more accurate data on the H-mode threshold power and on transport scaling close to this threshold.

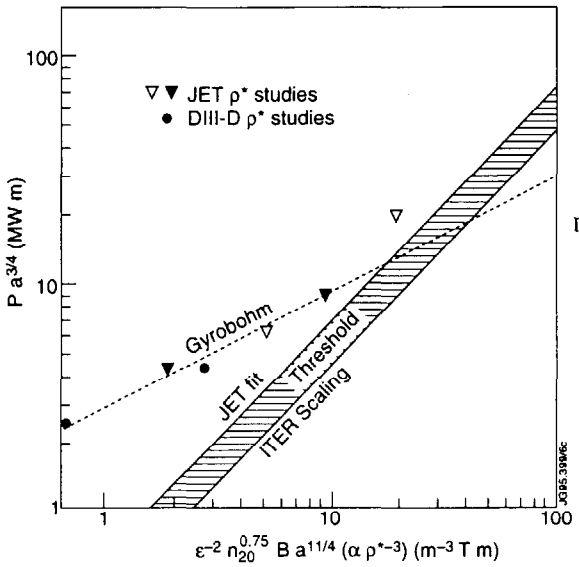

Figure 14. ρ* scaling data of energy confinement in relation to H-mode threshold power which can be interpreted in terms of gyrobohm scaling which degrades as H-mode threshold power is approached

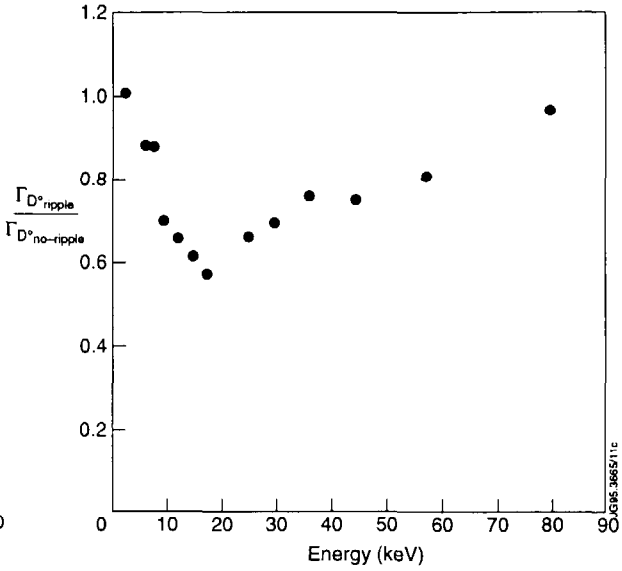

Figure 15. Effect of ripple on measured neutral particle fluxes showing that mainly particles with intermediate energies (thermal to 10's of keV) are affected whereas losses of thermal and high energy particles are very small

6. Fast particle confinement

Fast particle confinement has been addressed through toroidal field ripple experiments and studies of Alfvén Eigenmodes.

6.1. ITER specific toroidal field ripple experiments

The toroidal magnetic field ripple was varied in JET in the ITER-relevant range of 0.1% to 2% ripple at the plasma edge. These experiments [18] show a noticeable, but small effect of ripple on the H-mode and the sensitivity of the plasma to error field locked modes. Low levels of ripple (≈1% at edge) are found to improve H-mode confinement, probably due to the effect on ELM frequency, while high levels of ripple (>1.5% at edge) degrade H-mode confinement quality. High energy neutral particle flux measurements (figure 15) and triton burn-up experiments show that ripple induced losses of thermal and high energy particles (125keV NB ions and 1MeV tritons) are very small (a few %, or less) and are consistent with preliminary calculations of stochastic diffusion losses. The observed losses of intermediate energy particles (thermal to 10's of keV, see figure 15), however, are higher than predicted (from neoclassical theory).

6.2. Implications for ITER

In ITER, the ripple effects, in general, should be smaller than in JET (because of the smaller ρ* in ITER). The JET experiments indicate, therefore, that the ripple in ITER should have no significant effect on alpha-particle heating. The critical ripple issue for ITER remains, therefore, the heat load onto the first wall due to alpha-particle losses.

6.3. Alfvén eigenmode studies

Particle-wave interactions have the potential for increasing fast particle losses, thereby degrading alpha-particle heating and increasing the energetic alpha-particle produced wall damage. Alfvén Eigenmodes (TAE) have, therefore, been externally excited on JET using the in-vessel saddle coils or non-linear ICRF "beat" waves.

In TAE excitation experiments using the saddle coils, the Alfvén nature of the observed resonances has been verified by scanning the toroidal magnetic field. A strong multi-peak

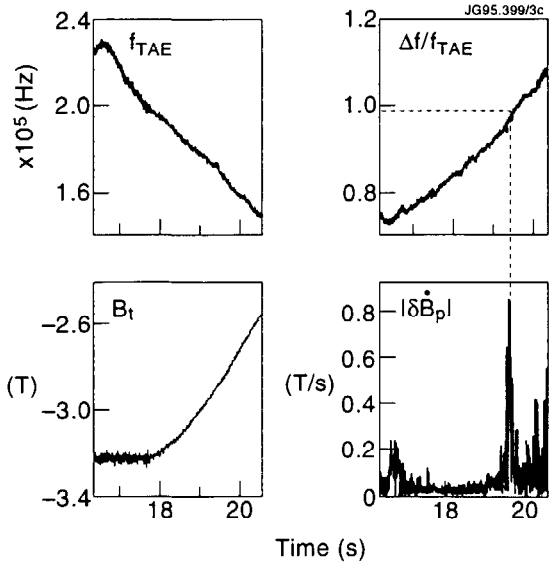

Figure 16. TAE excitation by ICRF beat waves

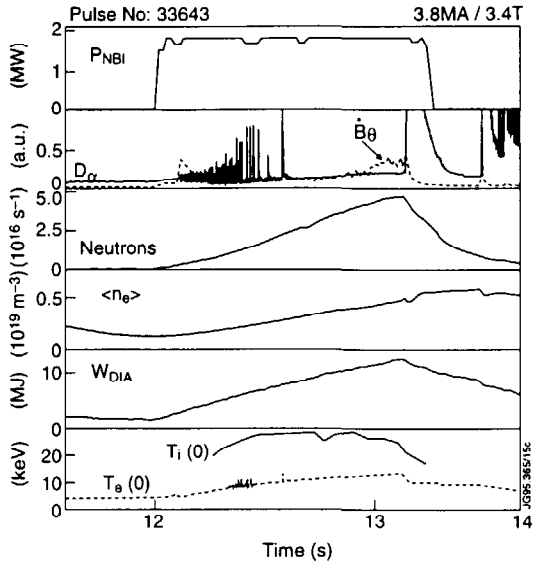

Figure 17. Pulse characteristics of the H-mode discharge that gave rise to the highest JET neutron rate in deuterium

structure has been seen with very weak damping $\gamma/\omega<10^{-3}$. These correspond to the first observation of kinetic Alfvén Eigenmodes [19].

The TAE resonance has also been excited when RF waves launched from two antennae differ in frequency (Δf) by the TAE frequency (f_{TAE}) and generate a "beat" wave as shown in figure 16 [20]. The TAE frequency was matched to Δf by scanning the toroidal field.

7. High fusion performance

JET currently pursues two routes to high fusion performance: steady-state ELMy detached divertor H-mode plasmas [21], the scenario envisaged for ITER, and transient ELM-free hot-ion H-mode plasmas [22], the regime that so far has produced the highest fusion performance in JET. In the latter case, performance increases as the duration of the ELM-free period is lengthened by reducing recycling (wall conditioning and/or use of the cryopump), increasing magnetic flux expansion in the divertor, and increasing magnetic shear (triangularity) at the plasma edge. These various methods of influencing the plasma behaviour are not independent and this complicates performance optimisation.

7.1. The highest performance in 1994/95

High fusion performance with $nT\tau_E$ values comparable to the best results of the past has been obtained during 1994/95, even though the plasma volume is now 20% smaller. Figure 17 shows an ELM-free hot-ion H-mode at 3.8MA/3.4T with 18MW of NBI and high flux expansion which has a neutron yield of $4.7x10^{16}s^{-1}$ (a new JET record in deuterium) and a fusion triple product $nT\tau_E > 8x10^{20}m^{-3}keVs$ (within 10% of previous best (see figure 18)). The high performance phase of this discharge is terminated by a "giant" ELM, simultaneous with a sawtooth, and preceded for ~200ms by high frequency MHD activity from the plasma core (radii $< r_{q=1}$). This MHD activity is observed on the magnetic pick-up coils and is seen to affect the central ion temperature and the neutron rate.

7.2. Limitations to high performance

In general, three classes of MHD phenomena can be involved in limiting the performance in hot-ion H-modes [23]: sawteeth and other internal MHD phenomena in the plasma centre;

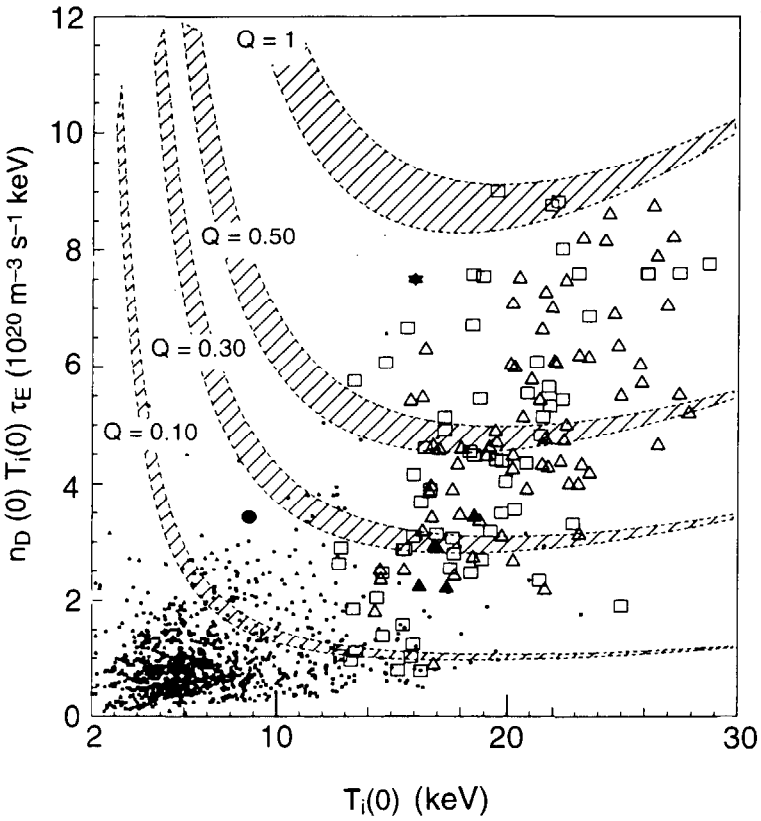

Figure 18. Fusion triple product plotted versus central ion temperature; Q contours are calculated referring to steady-state conditions. Symbols: Squares: 1991/92 data, Triangles: 1994/95 data (open symbols satisfy $T_i(0)>1.5T_e(0)$, solid symbols $dW/dT<0.1P_{in}$). Filled star: 1995 quasi-steady 'stepdown' discharge. Filled circle: ELMy 5MA H-mode.

and "outer" modes and "giant" ELMs in the plasma edge (figure 19). LHCD has been seen to control sawteeth and to soften the effect of the "outer" modes [24] but high performance plasmas are limited at a normalised $\beta_N \approx 1.8$, well below the Troyon limit ($\beta_N=2.8$) (figure 20).

On the other hand, quasi-steady-state stable operation has been produced with high normalised plasma pressure ($\beta_p>2$, $\beta_N>3$), high bootstrap current fraction (>50%) and H-mode confinement ($H_{89}>2.0$) [25] (figure 21).

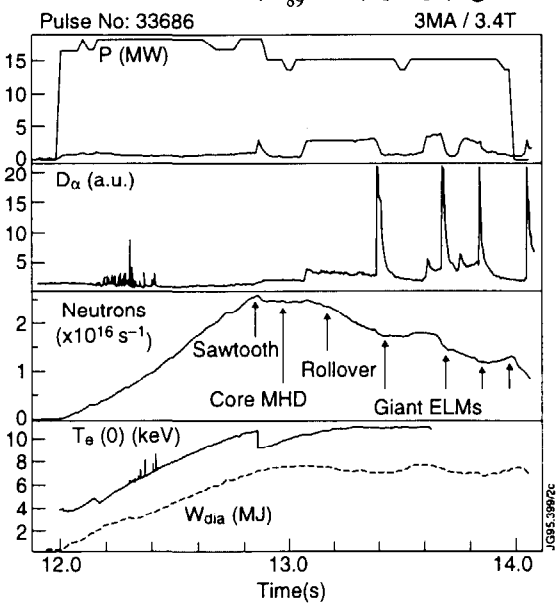

Figure 19. Pulse characteristics showing MHD phenomena that can limit high performance hot-ion H-modes: sawteeth and other internal MHD modes (centre) and "outer" modes and "giant" ELMs (edge)

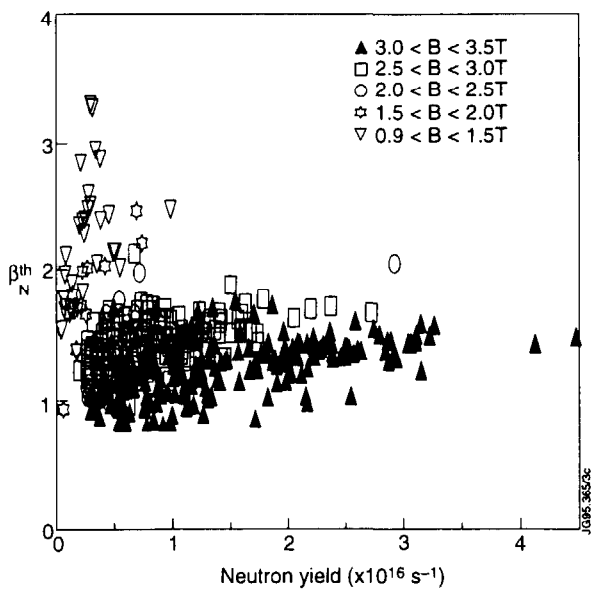

Figure 20.Relationship between normalised beta (=β/(I/aB)) and neutron rate for data from the 1994/95 campaign

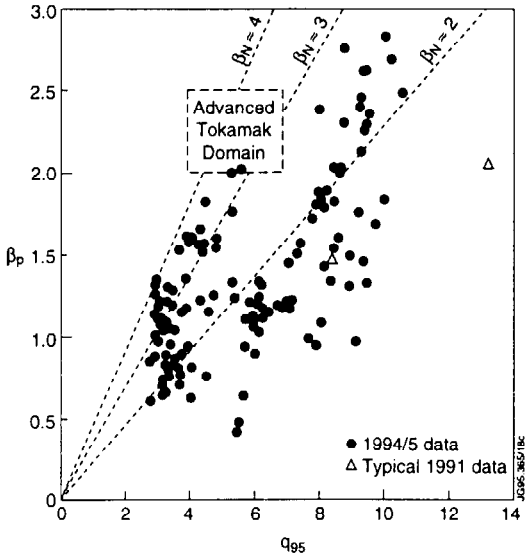

Figure 21. Experimental values of β_p versus edge safety factor q_{95} for quasi-steady state H-modes at low plasma currents

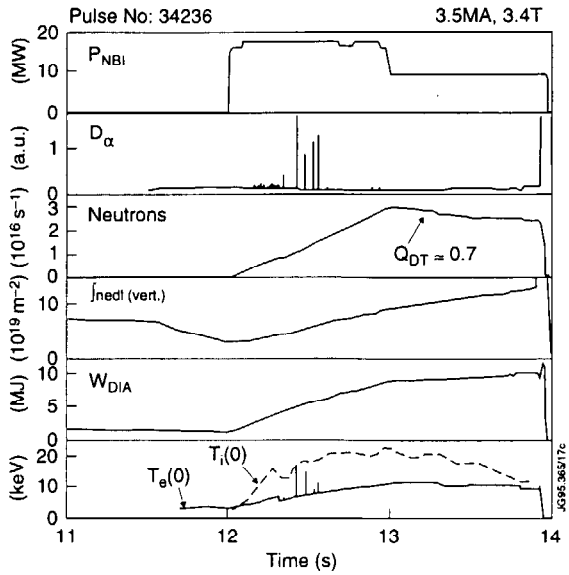

Figure 22. Pulse characteristics of quasi steady-state power "step-down" discharge Pulse No. 34236

These discharges at low plasma current can exceed the Troyon limit at high values of β_p, although the stored energy and neutron rate are low. This result implies that the pressure gradient in most of the plasma is well below that predicted by ideal ballooning mode theory. Stability calculations [26] confirm this, except close to the plasma edge where the experimental pressure gradients approach those predicted by theory. However, there is no evidence that ballooning modes are responsible for the "outer" modes or ELMs. Furthermore, kink stability analysis [27] suggests that the edge current density could be sufficient to destabilise external kink modes in hot-ion H-mode discharges and MHD data suggest that the terminating events do include an n=1 "kink".

7.3. High performance quasi-steady-state operation

It is possible to delay termination of the high-performance phase by reducing the NB power in order to remain just below the MHD stability limit. In this way, the neutron rate and diamagnetic stored energy remain high and in steady-state for up to 1s [28]. Such a power step-down experiment is shown in figure 22, where an equivalent Q_{DT} above 0.7 was maintained for almost 1s. In this discharge, the density continues to rise after the step-down, although the rate of increase is reduced (this was despite the attempt to minimise the density rise following the step-down by retaining mostly the high voltage 140kV beams). The increasing density facilitates the convergence of T_i and T_e but leads to a lower average temperature.

Heating systems can now be feedback controlled to maintain pre-set levels of stored plasma energy, neutron yield etc. and this will be exploited in the 1996 campaign.

7.4. Projected D-T performance

TRANSP D-T projections from Pulse No. 33643, under the assumption that the target plasma hydrogenic content is initially 50:50 D:T and that the 7MW of 140kV deuterium beams are replaced by tritium beams at the same power (the tritium power will actually be increased to 12.5MW in DTE1), indicate an equivalent $Q_{DT} \approx 1$, transiently, and $Q_{DT} > 0.7$ for 0.3s. In the same way, the power step-down experiment Pulse No. 34236 extrapolates to an equivalent $Q_{DT} > 0.7$ for 1s. As shown in figure 23, a substantial increase in the central electron temperature

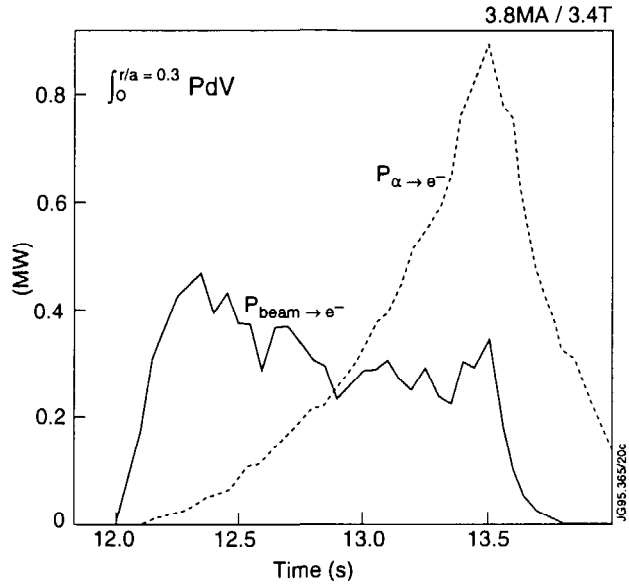

Figure 23. Comparison of central heating to electrons from α-particles and direct neutral beam heating from D-T TRANSP simulation of Pulse No.33643 (figure 17)

should result since the alpha-particle heating exceeds the direct electron heating from NBI. This offers good prospects for studying the effects of alpha-particle heating in the forthcoming DTE1 experiments.

7.5. Summary and prospects on JET

High fusion performance plasmas have been demonstrated in the new JET, in spite of a 20% reduction in plasma volume. Performance is limited by various MHD phenomena to $\beta_N \approx 1.8$, less than the Troyon value of 2.8. Benefits are expected to accrue prior to DTE1 from operating at higher toroidal magnetic field (4T), from the more closed Mark II divertor and, possibly, from current profile control.

8. Summary and conclusions

These results with the new JET have made significant contributions to the physics R&D for ITER and have highlighted the areas where future work should concentrate. They have also laid the foundation for the next phase of the JET Programme, ITER specific divertor studies with the more closed Mark IIA and Mark II Gas Box divertors in 1996 and 1997/98, respectively, and D-T experiments with up to 2×10^{20} neutrons (DTE1) starting in late 1996.

References

[1] Keilhacker M and the JET Team,1994, Proc. of ICPP - Invited Papers (Edited by P H Sakanaka and M Tendler) Published by American Institute of Physics

[2] Rebut P-H et al, 1993, *Fusion Engineering and Design* **22** 7

[3] Sartori R et al, 1995, *Europhysics Conference Abstracts (Proc. 22nd European Conference on Controlled Fusion and Plasma Physics), EPS, Bournemouth, U.K.* **Vol. 19C (Part IV)** 141

[4] Watkins M L and Rebut P-H, 1992 *Europhysics Conference Abstracts (Proc. 19th European Conference on Controlled Fusion and Plasma Physics), EPS, Innsbruck, Austria* **Vol. 16C (Part II)** 731

[5] Matthews G, 1995, *Proc. 22nd European Conference on Controlled Fusion and Plasma Physics, EPS, Bournemouth, U.K. (Invited Paper), this volume*

[6] Taroni A et al, 1994, *in Proc. of the Joint Lausanne-Varenna Workshop on the Theory of Fusion Plasmas, Varenna, Italy.*
[7] Weber S A et al ,*ibid*
[8] Reichle R et al, 1995 *Europhysics Conference Abstracts (Proc. 22nd European Conference on Controlled Fusion and Plasma Physics), EPS, Bournemouth, U.K.* **Vol. 19C (Part III)** 085
[9] The JET Team (presented by M L Watkins), 1994, *Plasma Physics and Controlled Fusion 36 B241*
[10] Janeschitz G, 1995 *Proc. 22nd European Conference on Controlled Fusion and Plasma Physics, EPS, Bournemouth, U.K. (Invited Paper), this volume*
[11] Tubbing B et al, 1995, *Europhysics Conference Abstracts (Proc. 22nd European Conference on Controlled Fusion and Plasma Physics), EPS, Bournemouth, U.K.* **Vol. 19C (Part III)** 457
[12] Igitkhanov Y et al, *ibid (**Part IV**) 317*
[13] Righi E et al, *ibid (**Part II**) 073*
[14] Ryter F et al, 1994, *Europhysics Conference Abstracts (Proc. 21st European Conference on Controlled Fusion and Plasma Physics), Montpellier, France* **Vol. 18B (Part I)** 334
[15] Balet B et al, 1995, *Europhysics Conference Abstracts (Proc. 22nd European Conference on Controlled Fusion and Plasma Physics), EPS, Bournemouth, U.K.* **Vol. 19C (Part I)** 009
[16] Greenfield C et al, 1994, *General Atomics Report GA-A21842*
[17] Petty C et al, 1995, *Physics of Plasma,* **Vol 2** *2342*
[18] Tubbing B et al,1995, *Europhysics Conference Abstracts (Proc. 22nd European Conference on Controlled Fusion and Plasma Physics), EPS, Bournemouth, U.K.* **Vol. 19C (Part IV)** 001
[19] Fasoli A F et al, 1994, *Proc. 15th IAEA Conference on Plasma Physics and Controlled Nuclear Fusion Research, Seville, Spain, (Post Deadline Paper)*
[20] Fasoli A F et al, 1995, *Europhysics Conference Abstracts (Proc. 22nd European Conference on Controlled Fusion and Plasma Physics), EPS, Bournemouth, U.K.* **Vol. 19C (Part III)** 081
[21] Stork D et al, *ibid (**Part II**) 125*
[22] Jones TTC, 1995, *Proc. 22nd European Conference on Controlled Fusion and Plasma Physics, EPS, Bournemouth, U.K. (Invited Paper), this volume*
[23] Smeulders P et al, 1995, *Europhysics Conference Abstracts (Proc. 22nd European Conference on Controlled Fusion and Plasma Physics), EPS, Bournemouth, U.K.* **Vol. 19C (Part IV)** 061
[24] Fischer B et al, *ibid (**Part III**) 365*
[25] Challis C D et al, *ibid (**Part II**) 069*
[26] Hender T C et al, *ibid (**Part I**) 029*
[27] Huysmans G et al, *ibid (**Part I**) 201*
[28] Marcus F B et al, *ibid (**Part II**) 053*

Acknowledgements
The author wishes to thank the many members of the JET Team who contributed to this paper, and in particular, ML Watkins, DJ Campbell, JG Cordey, C Gormezano, TTC Jones, GF Matthews, PJ Lomas, B Tubbing and GC Vlases for their contributions and clarifying discussions, and to BE Keen for his assistance in editing the paper.

Appendix I

THE JET TEAM

JET Joint Undertaking, Abingdon, Oxon, OX14 3EA, U.K.

J.M. Adams[1], P. Ageladarakis, B. Alper, H. Altmann, P. Andrew, S.Ali-Arshad, P. Bak[12], B.Balet, Y. Baranov[8], P. Barker, R. Barnsley[2], M. Baronian, D.V. Bartlett, A.C. Bell, G. Benali, E. Bertolini, V. Bhatnagar, A.J. Bickley, H. Bindslev, K. Blackler, D. Bond, T. Bonicelli, D. Borba, K. Borras[13], M. Brandon, P. Breger, H. Brelen, P. Brennan, W.J. Brewerton, T. Brown, M.L. Browne, T. Budd, M. Bures, A. Burt, P. Burton, T. Businaro, H. Buttgereit, M. Buzio, C. Caldwell-Nichols, D.J. Campbell, D. Campling, J. Candy[10], P. Card, G. Celentano, C.D. Challis, A.V. Chankin, A. Cherubini, D. Chiron, J. Christiansen, P. Chuilon, D. Ciric, R. Claesen, H.E. Clarke, S. Clement, J.P. Coad, I. Coffey[7], S. Cooper, J.G. Cordey, G. Corrigan, G. Cottrell, M. Cox[7], P. Crawley, R. Cusack, S. Dalla, N. Davies, S.J. Davies, J.J. Davis, N. de Benedetti, H. de Esch, J. de Haas, E. Deksnis, N, Deliyanakis, C. Deng[6], E. di Marchi, A. Dines, S.L. Dmitrenko, J. Dobbing, N. Dolgetta, S.E. Dorling, P.G. Doyle, H. Duquenoy, A.M. Edwards[7], A.W. Edwards, J. Egedal, J. Ehrenberg, A. Ekedahl[11], J. Ellis, M. Erba, S.K. Erents[7], L.G. Eriksson, H. Falter, R. Farengo, A. Fasoli[18], B. Fechner, B. Fischer, G. Fishpool, C. Froger, K. Fullard, M. Gadeberg, L. Galbiati, U. Gerstel[13], R. Giannella, A. Gibson, R.D. Gill, D. Godden, A. Gondhalekar, D. Goodall[7], C. Gormezano, R. Goulding[22], C. Gowers, J. Graham, K. Guenther, H. Guo[23], A. Haigh, B. Haist[4], C.J. Hancock, P.J. Harbour, N.C. Hawkes[7], N.P. Hawkes[1], J.L. Hemmerich, T. Hender[7], J. Hoekzema, L. Horton, J. How, A. Howman, M. Huart, G. Huysmans, A. Hwang, T.P. Hughes, F. Hurd, C. Ibbott, B. Ingram, M. Irving, J. Jacquinot, H. Jaeckel, J.F. Jaeger, O.N. Jarvis, F. Jensen, M. Johnson, E.M. Jones, L.P.D.F. Jones, T.T.C. Jones, J-F. Junger, F. Junique, A. Kaye, B.E. Keen, M. Keilhacker, W. Kerner, N.G. Kidd, Q.A. King, R. Konig, P. Kupschus, P. Lamalle[14], R. Lässer, J.R. Last, L. Lauro-Taroni, K. Lawson[7], M. Lennholm, J. Lingertat, A. Loarte, P.J. Lomas, M. Loughlin, T. Lovegrove, C. Lowry, E. Lyadina, A.C. Maas[15], B. Macklin, C.F. Maggi[16], M. Mantsinen[5], V. Marchese, F. Marcus, J. Mart, D. Martin, T. Martin, G. Matthews, H. McBryan, G. McCormick[13], P.A. McCullen, A. Meigs, F. Milani, J. Mills, R. Mohanti, R. Monk[17], P. Morgan, D. Muir, G. Murphy, F. Nave[21], G. Newbert, F. Nguyen[3], P. Nielsen, P. Noll, W. Obert, D. O'Brien, E. Oord, R. Ostrom, M. Ottaviani, S. Papastergiou, V.V. Parail, W. Parsons, B. Patel, A. Paynter, A. Peacock, N. Peacock[7], R.J.M. Pearce, G. Pereverzev[13], C. Perry, M.A. Pick, J. Plancoulaine, O. Pogutse, J-P. Poffé, L. Porte, R. Prentice, P. Prior, S. Puppin, G. Radford[9], T. Raimondi, R. Reichle, E. Righi, F. Rimini, A. Rolfe, A. Rookes[12], R.T. Ross, A. Rossi, L. Rossi, G. Sadler, G. Saibene, M. Salisbury[12], G. Sanazzaro, A. Santagiustina, F. Sartori, R. Sartori, R. Saunders, P. Savrukhin, M. Scibile, P. Schild, M. Schmid, B. Schunke, S.M. Scott, S. Sharapov, A. Sibley, R. Simonini, A.C.C. Sips, P. Smeulders, O. Smith[12], P. Smith, R. Smith, F. Söldner, M. Stamp, P. Stangeby[20], D.F. Start, C.A. Steed, D. Stork, P.E. Stott, A. Stuart, P. Stubberfield, D. Summers, H. Summers[19], W. Suverkropp, L. Svensson, P. Svensson, A. Tabasso[12], M. Tabellini, J. Tait, A. Tanga, A. Taroni, C. Terella, P.R. Thomas, K. Thomsen, B. Tubbing, H. van der Beken, P. van Belle, R. van der Linden, G. Vayakis, M. Verrechia, G. Vlases, M. von Hellermann, T. Wade, R. Walton, D. Ward, M.L. Watkins, N. Watkins[1], M.J. Watson, J. Wesson, M. Wheatley, D. Wilson, T. Winkel, C. Woodward, D. Young, I.D. Young, Q. Yu[6], F. Zannelli, L. Zannelli, K-D. Zastrow, N. Zornig, G. Zullo, W. Zwingmann.

PERMANENT ADDRESSES

1. UKAEA, Harwell, Didcot, Oxon, UK.
2. University of Leicester, Leicester, UK.
3. CEA, Cadarache, France.
4. KFA, Jülich, Germany.
5. Helsinki University of Technology, Espoo, Finland.
6. Institute of Plasma Physics, Hefei, P R of China.
7. UKAEA Culham Laboratory, Abingdon, Oxon, UK.
8. A.F. Ioffe Institute, St. Petersburg, Russia.
9. Institute of Mathematics, University of Oxford, UK.
10. Institute for Fusion Studies, University of Texas, Austin, Texas, USA.
11. Royal Institute of Technology, Stockholm, Sweden.
12. Imperial College, University of London, UK.
13. Max Planck Institut für Plasmaphysik, Garching, Germany.
14. Plasma Physics Laboratory, ERM-KMS, Brussels, Belguim.
15. FOM Instituut voor Plasmafysica, Nieuwegein, The Netherlands.
16. Dipartimento di Fisica, University of Milan, Milano, Italy.
17. Royal Holloway College, University of London, UK.
18. EPFL, Lausanne, Switzerland.
19. University of Strathclyde, 107 Rottenrow, Glasgow, UK.
20. Institute for Aerospace Studies, University of Toronto, Canada.
21. LNETI, Savacem, Portugal.
22. Oak Ridge National Laboratory, Oak Ridge, Tenn., USA.
23. INRS-Energieet Materiaux, Univ. du Quebec, Canada.

At July, 1995